JETIR.ORG ISSN: 2349-5162 | ESTD Year : 2014 | Monthly Issue
JOURNAL OF EMERGING TECHNOLOGIES AND INNOVATIVE RESEARCH (JETIR)
An International Scholarly Open Access, Peer-reviewed, Refereed Journal

Biosynthesis of Magnetic Iron Oxide Nanoparticle and Study of its Electrical Propertiesthrough Thin Film.

Vipin Kumar* &Ajay Kumar**
*Professor, Deptt of Physics, SKD University, Hanumangarh
**Research Scholar at Deptt of Physics, SKD University, Hanumangarh
** Asst. Prof., Department of Physics,Dr. B.R.A Govt. College Sriganganagar
Corresponding author: A Kumar (ajayghoran92@gmail.com)

Highlights

- Gamma iron oxide NPs have been synthesized using leaf extract from the Dalbergia sissoo tree by a green synthesis route.
- X-ray Diffraction (XRD) and Fourier Transform Infrared Spectroscopy (FTIR) studies confirmed that the bulk material produced was comprised only of nanocrystalline γ-Fe_2O_3 (phase pure).
- The phytochemicals in the leaf extract were used to stabilize and encapsulate the NPs, providing stability and functional surface features to the NPs.
- Thin films of γ-Fe_2O_3 produced by drop casting resulted in uniform, defect-free thin film materials.
- Thin films exhibited ohmic conduction behavior and a negative temperature coefficient.
- The low activation energy suggests that the conduction mechanism is thermally assisted hopping conduction.

Abstract

The use of plants to make functional nano materials provides an environmentally friendly manner to produce these materials. In this study, γ-Fe_2O_3 nanoparticle biosynthesis has been achieved using the leaf extract of Dalbergia sissoo. The phytochemicals present in the leaf extract served as both reducing and stabilizing agents during the formation of the nanoparticles. The characterization of the nanoparticles using X-ray diffraction indicated that they are a cubic spinel material and contain an average crystallite size of 11.3 nanometres. The structural characterization of the nanoparticles using Fourier Transform Infrared Spectroscopy showed Fe-O lattice vibrations and the surface of the nanoparticles contained organic functional surface groups. The characterization of the nanoparticles using Field Emission Scanning Electron Microscopy showed quasi-spherical formation and limited number of agglomerated nanoparticles as a result of annealing. The characterization of the nanoparticles using Ultraviolet-Visible Spectroscopy demonstrated that they have a strong ultraviolet light absorbance and potential of photocatalytic properties. Evaluation of the direct and indirect band gap through characterization of the nanoparticles indicated that quantum confinement effects are present. The production of thin films through drop casting of the nanoparticles exhibit a smooth morphology. Electrical characterization of the thin films demonstrated linearly behaving–current voltage characteristics in addition to dependence upon temperature with regard to their conductivity. Arrhenius analysis resulted in determining low activation energy (0.1736 eV) for the electrical behaviour of the thin films produced in this study. The results obtained in this study suggest that the biosynthesized γ-Fe_2O_3 nanoparticles display properties suited for use in various sensing, photocatalytic functions, and for use in low-temperature electronic applications.

Keywords: Green synthesis; γ-Fe_2O_3 nanoparticles; *Dalbergia sissoo*; Thin films; Electrical conductivity; Activation energy.

1. Introduction:

Nanomaterials have at least one of dimensions in the range of 1–100 nm. Since at this range of size quantum effects begin to dominate, these materials show different kinds of physical, chemical, electrical, and mechanical properties compared to their bulk form. A controlled synthesis can produce nanomaterials with desired properties. They have diverse applications

in the fields of electronics, medicine, energy storage, and environment (Baig et al., 2021). Nanotechnology deals with the control and manipulation of the properties of materials at the nano scale. Nanotechnology originated from visionary ideas, notably Richard Feynman's 1959 lecture *"There's Plenty of Room at the Bottom,"* which proposed atomic-scale manipulation of matter. The term nanotechnology was later coined by Norio Taniguchi in 1974 to describe nanoscale precision manufacturing. Nanotechnology is not new for humans; evidence indicates that ancient people used this technology in many ways. The famous Lycurgus cup, Damascus sword, and medieval church colorful window glasses are some examples (Bayda et al., 2020; Freestone et al., 2007; Reibold et al., 2006).

Dalbergia sissoo Roxb. (Family: Fabaceae), commonly known as Shisham in the Sri Ganganagar region of Rajasthan, is a deciduous tree native to the Indian subcontinent. The plant is rich in bioactive phytochemicals such as flavonoids, phenolics, and tannins, which possess antioxidant and antimicrobial activities. Traditionally, *D. sissoo* has been used in herbal medicine for treating inflammation, skin disorders, and gastrointestinal ailments, while its wood is extensively utilized in furniture and construction industries. The presence of reducing and stabilizing biomolecules makes *D. sissoo* a suitable biological resource for green synthesis of nanoparticles (Bhattacharya, Singh &Ramrakhyani, 2014; Johnson et al., 2024; Yasmeen & Gupta, 2021).

Metal oxide nanoparticles constitute an important class of functional materials due to their structural stability, tunable electronic properties, and chemical reactivity. Metal oxide nanoparticles are known for their superior catalytic properties due to their small size and large surface area (Khezri& Vahdat, 2025). Studies also exhibit their electrochemical properties, making them suitable for electrocatalysis, sensors, energy storage, biomedical applications, and fuel cells (Alduhaidahawia &Alantaki, 2025; Boshoman et al., 2023; Rezić, 2022; Sale et al., 2022; Steinhauer, 2021; Abuzeid et al., 2023).

Green synthesis is a novel method and is gaining popularity in the research field. This method is non-toxic, environmentally friendly, and cost-effective. In this method, plants, algae, fungi, bacteria, and yeast are used to synthesize nanoparticles. Phytochemicals, bioactive proteins, enzymes, polysaccharides, etc., act as reducing and capping agents. Green-synthesized nanoparticles exhibit improved biocompatibility, cost-effectiveness, and environmental safety, making this method highly suitable for scalable and sustainable nanomaterial production (Boroumand Moghaddam et al., 2015; Karunakaran et al., 2023; Kulkarni et al., 2023;Abuzeid et al., 2023).

2.Materials and Methods:

2.1 Materials:

Iron precursor salt ferrous sulphate heptahydrate $FeSO_4.7H_2O$ and sodium hydroxide (NaOH) pellets were purchased from Loba Chemie Pvt. Ltd., India. Deionized water with total dissolved solids (TDS) below 10 ppm was used throughout the experiments without further purification.

2.2Preparation of plant leaf extract

Fresh leaves of *D. sissoo* (Shisham) were taxonomically authenticated by Dr. Rajendra Kadwasra, Professor, Department of Botany, Dr. Bhimrao Ambedkar Government College, Sri Ganganagar, Rajasthan, India. The leaves were collected from the botanical garden of the college and thoroughly washed with distilled water to remove dust and other impurities, and cut into fine pieces.

Approximately 10g of chopped leaves were boiled in 100 mL of distilled water at 60 °C for 30–45 minutes under continuous heating. The resulting mixture was first filtered through a stainless-steel strainer to remove coarse residues and then re-filtered using Whatman filter paper No. 1. A clear yellowish-brown plant extract was obtained, stored in clean glass bottles, and preserved at 4 °C for further use.

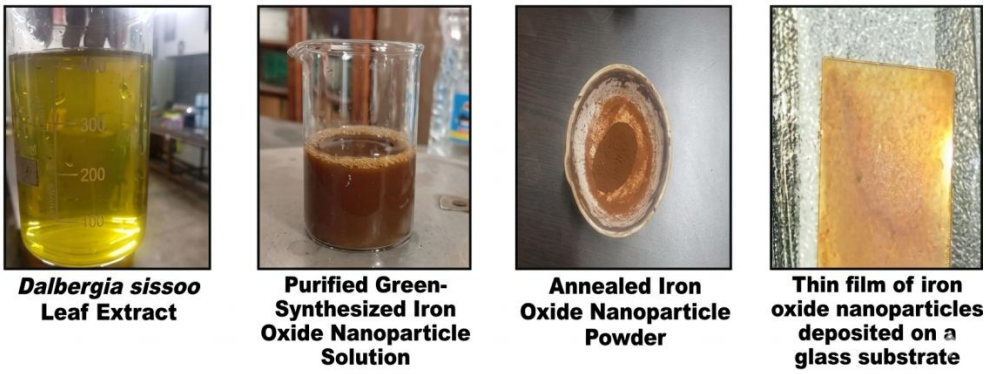

Figure 1: Stepwise green synthesis of iron oxide nanoparticles and thin-film formation

2.3 Green synthesis of iron oxide nanoparticles

For nanoparticle synthesis, 350 mL of deionized water was taken in a 500 mL beaker, and the optimized concentration of precursor salt (1 mM) was dissolved in it. Subsequently, 90 mL of *D. sissoo* leaf extract was added dropwise. The pH of the reaction mixture was adjusted to the optimized value of 9 using freshly prepared 0.5 N NaOH solution.

The reaction mixture was incubated at 25 °C for 48 hours. A gradual color change of the solution from yellowish to blackish brown, followed by the formation of blackish precipitate, indicated the formation of iron oxide nanoparticles. The precipitate was collected by centrifugation at 5000 rpm for 20 minutes, and the supernatant was discarded. The centrifugation process was repeated 3–4 times with distilled water and absolute ethanol to remove unreacted precursors and residual plant extract. The purified precipitate was then dried at a constant temperature of 50 °C overnight. A brownish black (Karami, 2010) color powder was obtained and ground using a mortar and pestle to make a fine powder. The powder was annealed at 320 °C for 1.5 hours to enhance phase purity and crystallinity. The annealed iron oxide nano powder was brownish red and ground again to make a fine powder using a pestle–mortar. It was stored in airtight medical sample vials for further analysis.

2.4 Fabrication of iron oxide thin films by drop-casting method

Thin films of iron oxide nanoparticles were fabricated using the classical drop-casting technique. To obtain homogeneous nanoparticle dispersion without employing probe sonication, approximately 0.5 mL of the synthesized nanoparticle suspension was taken in a centrifuge tube and mixed with 5 ml solvent of 30% ethanol and 70% distilled water. The mixture was centrifuged at 4000 rpm until the supernatant became clear, allowing larger agglomerated particles to settle at the bottom.

Approximately 3mL of the clear supernatant containing well-dispersed nanoparticles was collected for thin-film deposition. Glass substrates were cut into 1 cm × 1 cm pieces and cleaned successively with distilled water, ethanol, and acetone to remove surface contaminants. To introduce controlled surface roughness and improve film adhesion, the substrates were immersed in 0.5 M HNO_3 for 3 hours, this treatment did not alter the optical transparency or reflectance of the glass. The cleaned substrates were placed on a hot plate maintained at 60°C. Using a micropipette, a single drop of the nanoparticle dispersion was deposited onto the heated substrate. Each drop required approximately 25 min to dry completely, enabling slow solvent evaporation and significantly minimizing the coffee-ring effect. This procedure was repeated for 20 successive drops, resulting in a smooth, uniform, and crack-free thin film (Arulkumar &Thanikaikarasan, 2023; Marica et al., 2023).

The deposited iron oxide thin films were finally annealed at 320 °C for 2 h to enhance crystallinity and electrical stability. The electrical properties of the iron oxide nanoparticle thin films were subsequently investigated.

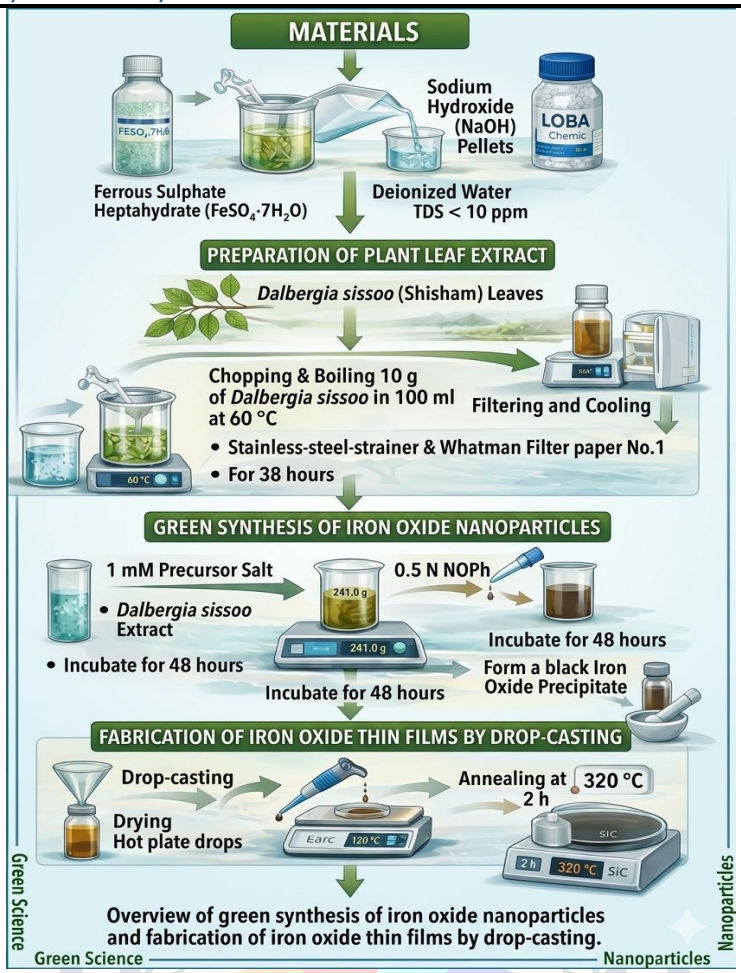

Figure 2: Green synthesis and thin-film fabrication workflow of iron oxide nanoparticles

3. Result and discussion:

3.1 XRD analysis: X-ray diffraction (XRD) analysis was carried out at CIF,BITS Pilani using a Bruker D2 Phaser diffractometer with Cu Kα radiation (λ = 1.5406 Å). The diffraction pattern exhibited characteristic peaks at 2θ = 30.62°, 35.97°, 43.60°, 54.05, 57.68°, and 62.97°, which are in agreement with the standard JCPDS/ICDD card no. 00-039-1346, confirming the formation of the cubic spinel maghemite (γ-Fe_2O_3) phase. Similar diffraction features for γ-Fe_2O_3 have been reported in earlier studies (Biswas et al., 2024; Layek et al., 2010; Darezereshki, 2010; Yadav et al., 2023; Alagiri & Hamid, 2014;Ogholbeyg et al., 2018).

The dominance of intense diffraction peaks corresponding to γ-Fe_2O_3 indicates its magnetic nature and high phase purity. However, the presence of a few weak additional reflections after peak refinement suggests the existence of a trace amount of hematite (α-Fe_2O_3) as a secondary phase. The average crystallite size of the synthesized Fe_2O_3 nanoparticles was estimated using the Debye–Scherrer equation: $D = \frac{k\lambda}{\beta \sin\theta}$ where D is the crystallite size, k is the shape factor (0.9), λ is the wavelength of Cu Kα radiation, β is the full width at half maximum (FWHM) of the diffraction peak (in radians), and θ is the Bragg diffraction angle. The crystallite sizes calculated from different diffraction peaks are summarized in Table 1.1.

Table 1.1: XRD analysis summary

2θ (deg)	θ (deg)	FWHM (deg)	β (rad)	βcosθ	4sinθ(X-axis)	Scherrer Size (D nm)
30.62	15.31	0.7493	0.013078	0.012614	1.0562	10.99 nm
35.97	17.98	0.6209	0.010836	0.010307	1.2354	13.45 nm
43.60	21.80	0.7510	0.013108	0.012171	1.4855	11.39 nm
54.05	27.02	0.8509	0.014851	0.013229	1.8178	10.48 nm
57.68	28.84	0.6898	0.012039	0.010545	1.9297	13.15 nm

The XRD analysis revealed the uniform growth of nanocrystalline iron oxide, with an average crystallite size of 11.3 nm. A gradual decrease in crystallite size at higher diffraction angles was observed, which indicates the presence of internal microstrain and lattice imperfections within the crystal structure.

Figure 3: XRD patterns of iron oxide nanoparticles: **(A)** experimental (original) pattern and **(B)** refined pattern.

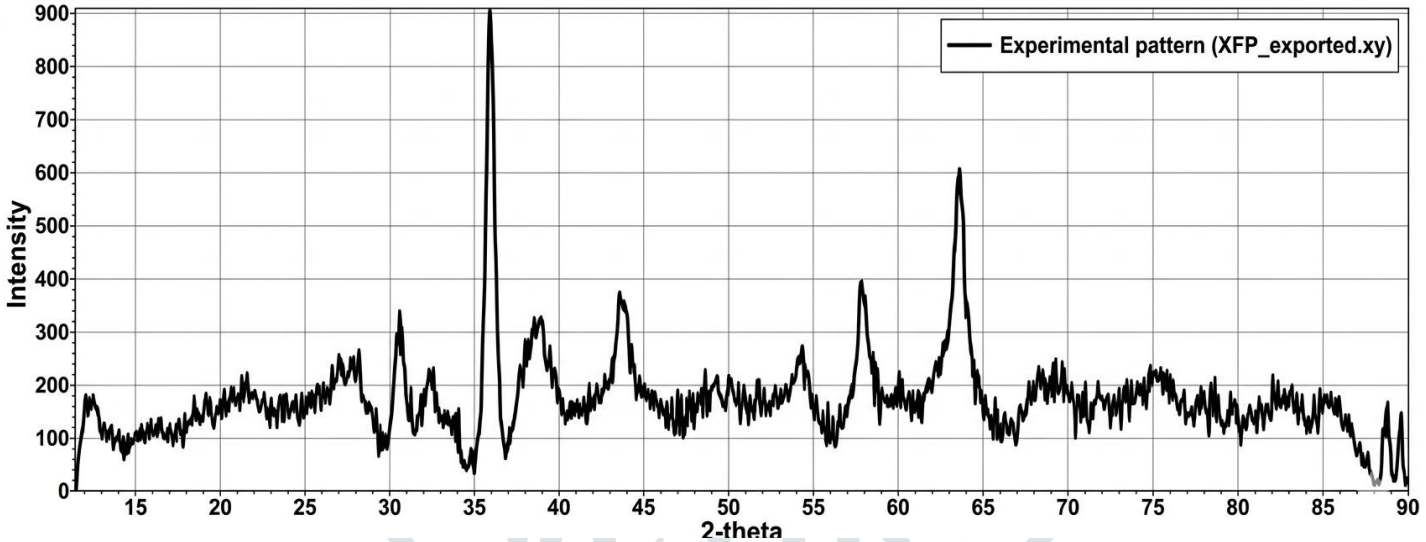

(A)

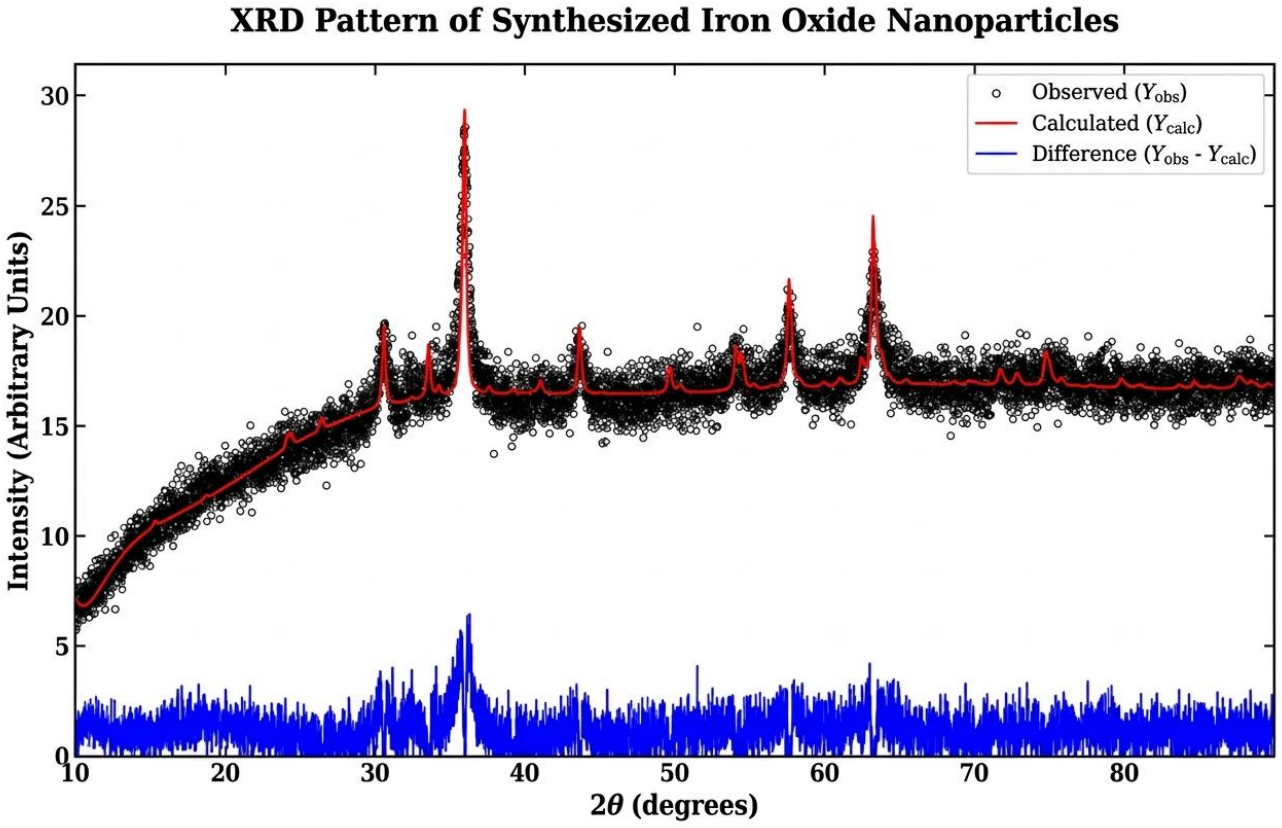

(B)

3.2 FTIR Analysis and Phytochemical Capping of Iron Oxide Nanoparticles

FIGURE 4: FTIR of synthesized iron oxide nanoparticles

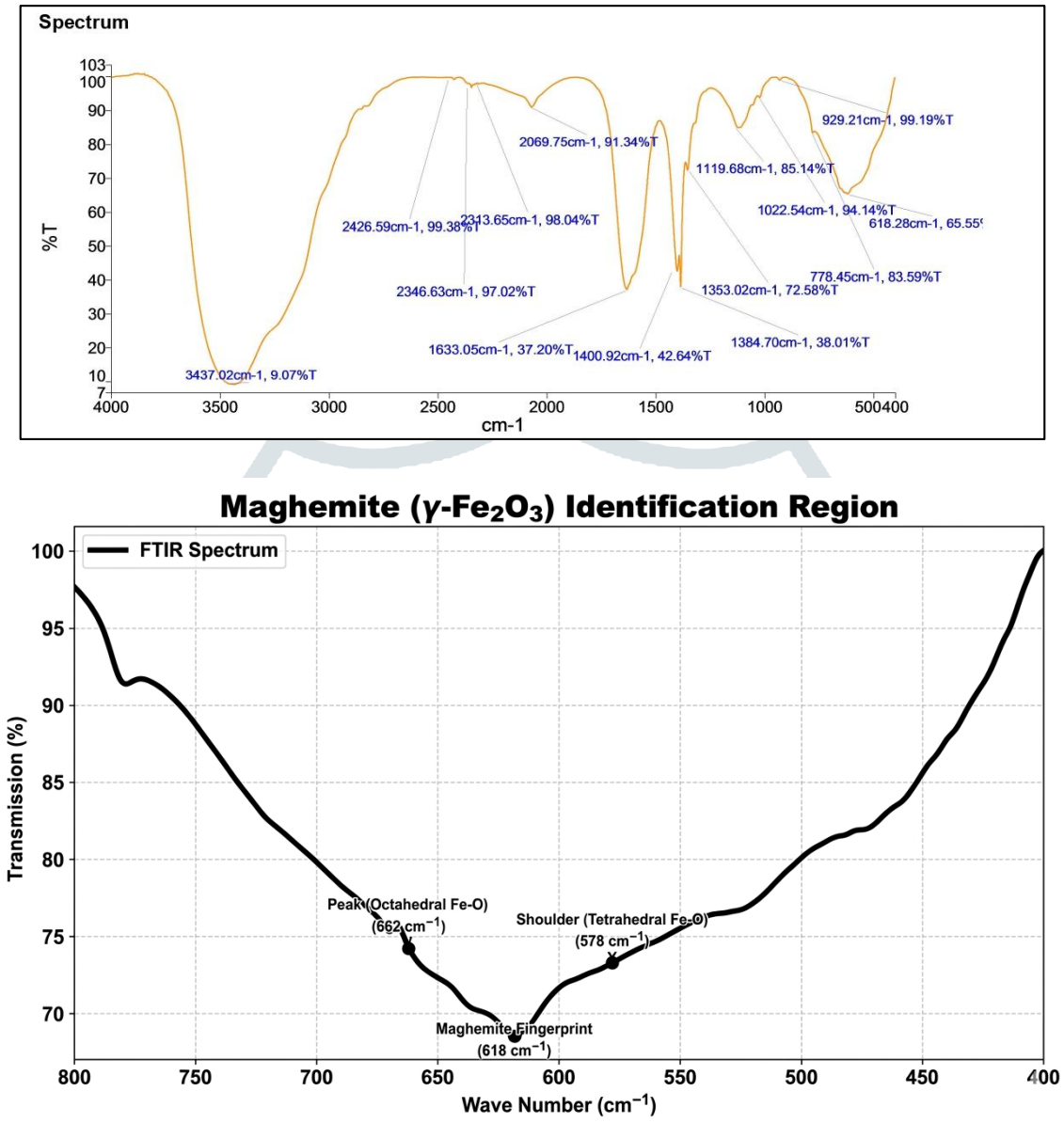

Fourier transform infrared (FTIR) spectroscopy was employed to identify the molecular fingerprint and to characterize both the iron oxide lattice vibrations and the plant-derived organic functional groups involved in nanoparticle formation and stabilization. The FTIR spectrum exhibited a strong absorption region between 400 and 800 cm^{-1}, which is characteristic of Fe–O stretching vibrations in spinel-structured iron oxides. A prominent absorption band observed at 618 cm^{-1} corresponded to the fingerprint vibration of γ-Fe_2O_3 (maghemite), distinguishing it from hematite (α-Fe_2O_3). The shoulder at 578 cm^{-1} and the peak at 662 cm^{-1} were assigned to Fe–O vibrations at tetrahedral and octahedral sites, respectively, within the maghemite lattice. The presence of a broadened absorption feature around 618 cm^{-1} suggested overlapping Fe–O stretching and bending modes, indicating the possible coexistence of hematite as a minor secondary phase. These FTIR observations were consistent with the XRD results, confirming the formation of predominantly nanocrystalline maghemite iron oxide. Further analysis of the FTIR spectrum revealed the involvement of phytochemicals from the plant extract as reducing, capping, and stabilizing agents. A broad and intense absorption band in the range of 3385–3437 cm^{-1} was attributed to –OH stretching vibrations, indicating a high abundance of hydroxyl groups associated with phenols, flavonoids, and alcohols. These functional groups acted as the primary reducing agents, facilitating the conversion of ferrous ions into γ-Fe_2O_3 nanoparticles, and subsequently remained adsorbed on the nanoparticle surface, providing effective stabilization. The absorption bands observed in the 2920–3000 cm^{-1} region, with distinct peaks near 2921 cm^{-1} and 2850 cm^{-1}, were assigned to asymmetric and symmetric C–H stretching vibrations, which are characteristic of terpenoids, saponins, and fatty acids present in the plant extract. The band at 1625–1632 cm^{-1} was attributed to C=O stretching of amide groups or C=C stretching of aromatic rings, indicating the possible involvement of proteins and aromatic flavonoids in nanoparticle

capping. Additionally, the absorption band at ~1385 cm^{-1} was associated with C–N stretching or nitrate residues, while the band at ~1106 cm^{-1} corresponded to C–O stretching vibrations of polysaccharides and sugars. Overall, the FTIR analysis confirmed that the synthesized iron oxide nanoparticles were surface-functionalized with a complex mixture of plant-derived phytochemicals, including phenolics, flavonoids, terpenoids, polysaccharides, and proteins from *D. sissoo* leaf extract. The presence of these bioactive surface moieties not only enhanced nanoparticle stability but also increased their potential suitability for biomedical and environmental applications. The FTIR findings were in good agreement with previously reported studies (Alshamsi& Hussein, 2018; Singh et al., 2008; Darezereshki et al., 2010; Morales Morales, 2017; Singh et al., 2012)

3.3 Energy-Dispersive X-ray Spectroscopy (EDS) Analysis

FIGURE 5: EDS mapping of elements for synthesized iron oxide nanoparticle

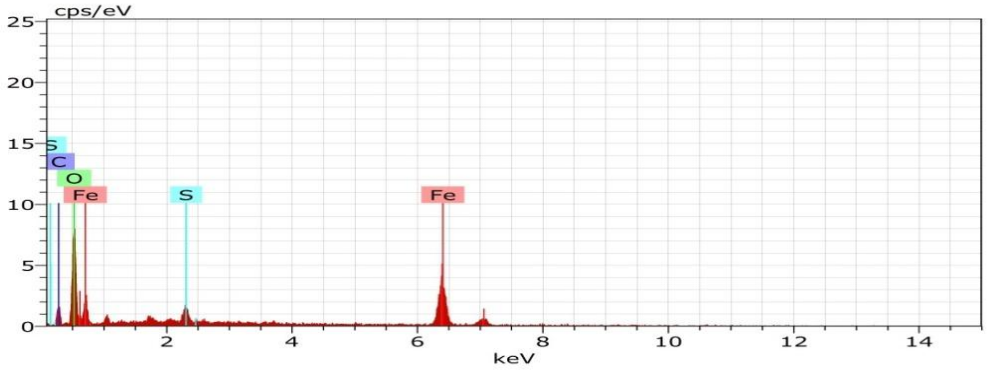

Spectrum: test 22240

Element	Series	unn. C [wt.%]	norm. C [wt.%]	Atom. C [at.%]	Error (3 Sigma) [wt.%]
Iron	K-series	47.28	56.17	25.65	5.03
Oxygen	K-series	24.61	29.23	46.60	12.69
Carbon	K-series	10.23	12.15	25.80	8.39
Sulfur	K-series	2.07	2.45	1.95	0.42
	Total:	84.18	100.00	100.00	

The elemental composition of the green-synthesized iron oxide nanoparticles was examined using energy-dispersive X-ray spectroscopy (EDS). The EDS spectrum exhibited a strong characteristic Kα peak of iron (Fe) at 6.40 keV and a distinct Kα peak of oxygen (O) at 0.52 keV, confirming that the synthesized material is composed primarily of iron and oxygen.Quantitative analysis revealed an atomic ratio of Fe:O 2:2.76, which is very close to the theoretical stoichiometric ratio of 2:3 for Fe_2O_3, indicating the successful formation of iron oxide nanoparticles. In addition, a weak signal corresponding to carbon (C) was detected, which can be attributed to phytochemical capping and stabilizing agents originating from the plant extract, consistent with the FTIR results. No additional elemental peaks were observed in the EDS.

3.3FESEM Analysis:

FIGURE 6:FESEM images of synthesized iron oxide nanoparticle

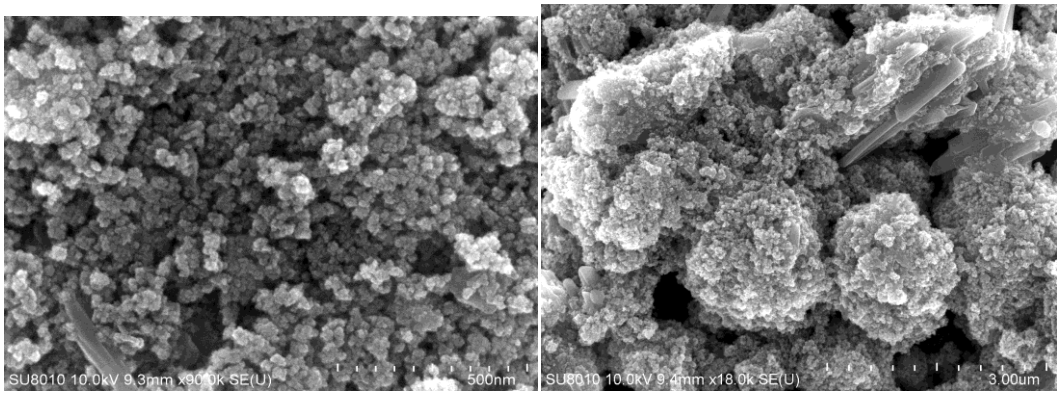

(A) After annealing

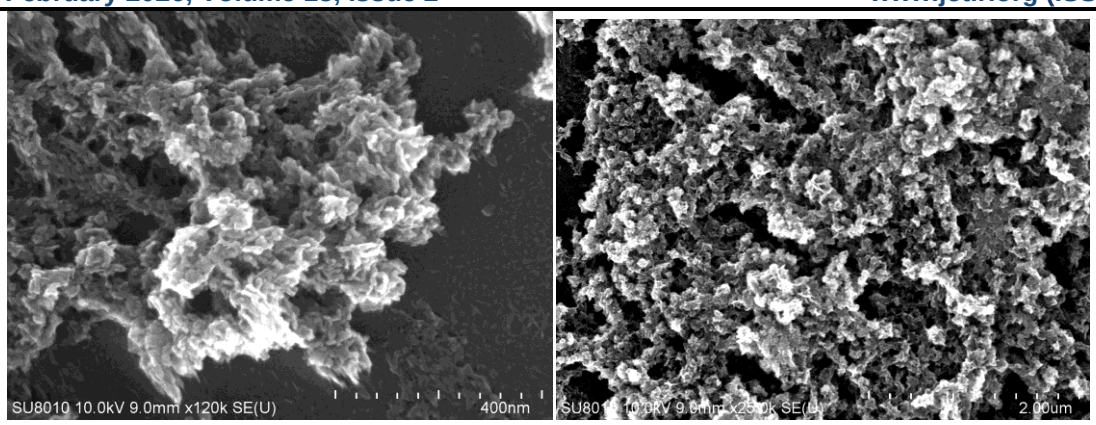

(B) Before annealing

Field Emission Scanning Electron Microscope (FESEM) images of the as-prepared γ-Fe_2O_3 nanoparticles showed nearly spherical to irregular particles with significant agglomeration and porous clusters, which is attributed to high surface area and magnetic interactions. The particle distribution appeared non-uniform with indistinct grain boundaries, indicating poor crystallinity. After annealing at 320 °C for 1.5 h, the nanoparticles became more quasi-spherical with improved grain boundaries and a relatively uniform size distribution. These morphological changes align well with XRD results, which show peak sharpening and enhanced intensity after annealing. Overall, annealing improved the structural ordering and compactness of the γ-Fe_2O_3 nanoparticles.

3.3.1 Analysis of Particle Size Distribution: The mean particle size obtained from FESEM measurements was **16.92 nm**, which is larger than the crystallite size calculated from XRD (**11.63 nm**). This discrepancy is expected and indicates that the XRD value represents the coherent scattering domain (crystallite size), while the FESEM-derived mean size reflects the actual physical particle size. The observed difference (5 nm) can be attributed to a surface layer or disordered region where atoms are not perfectly aligned in the crystal lattice.

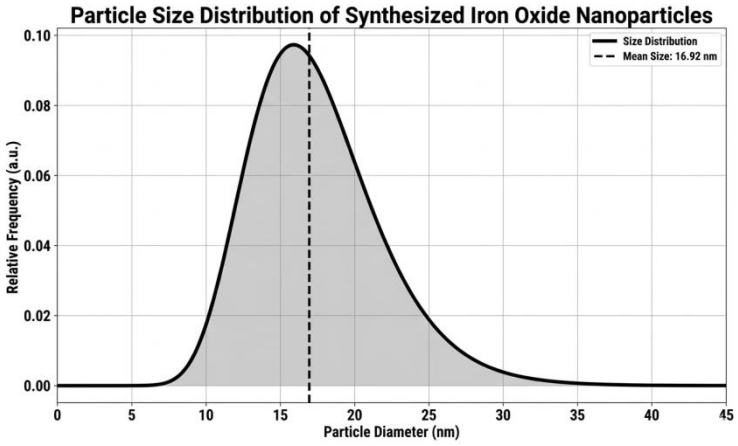

Figure 7: FESEM-derived particle size distribution of iron oxide nanoparticles showing larger mean size than XRD crystallite size

The relatively narrow size distribution and close agreement between crystallite and particle sizes suggest that the synthesized γ-Fe_2O_3 nanoparticles are largely single crystalline, rather than being composed of multiple crystallites agglomerated into larger particles.

3.4 UV–Vis Spectral Analysis:

The UV–Vis spectrum of the synthesized material was recorded using a Jasco Spectrophotometer (200–850 nm). A strong absorption band was observed in the UV region (200–320 nm), attributed to charge transfer transitions between O^{2-} and Fe^{3+} ions. The absorbance gradually decreased toward the visible region, indicating semiconductor-type behavior. Strong absorption in UV region suggested its potential applicability in photocatalytic and optoelectronic devices.

Figure 8: UV-Vis spectrum of synthesized iron oxide nanoparticle, tuac's plot for direct and indirect band gap.

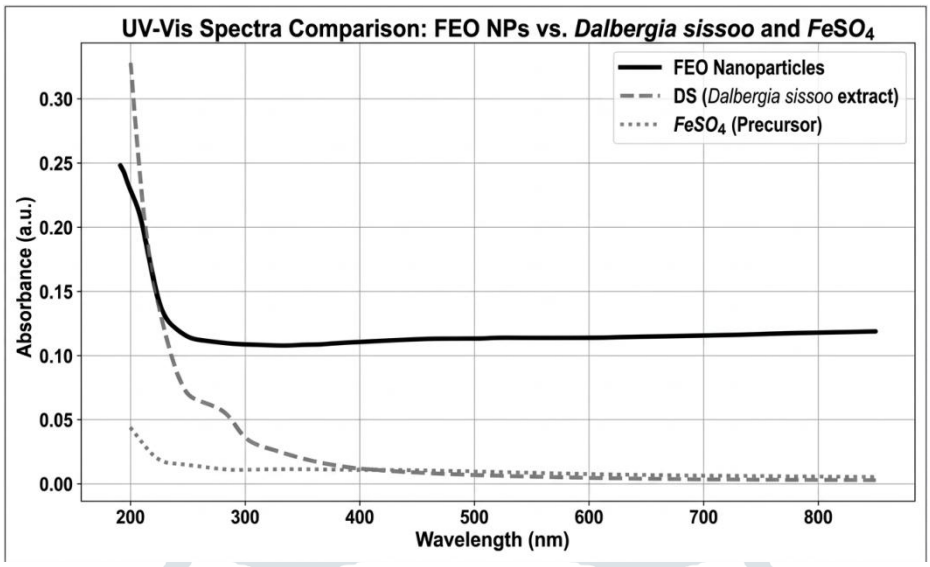

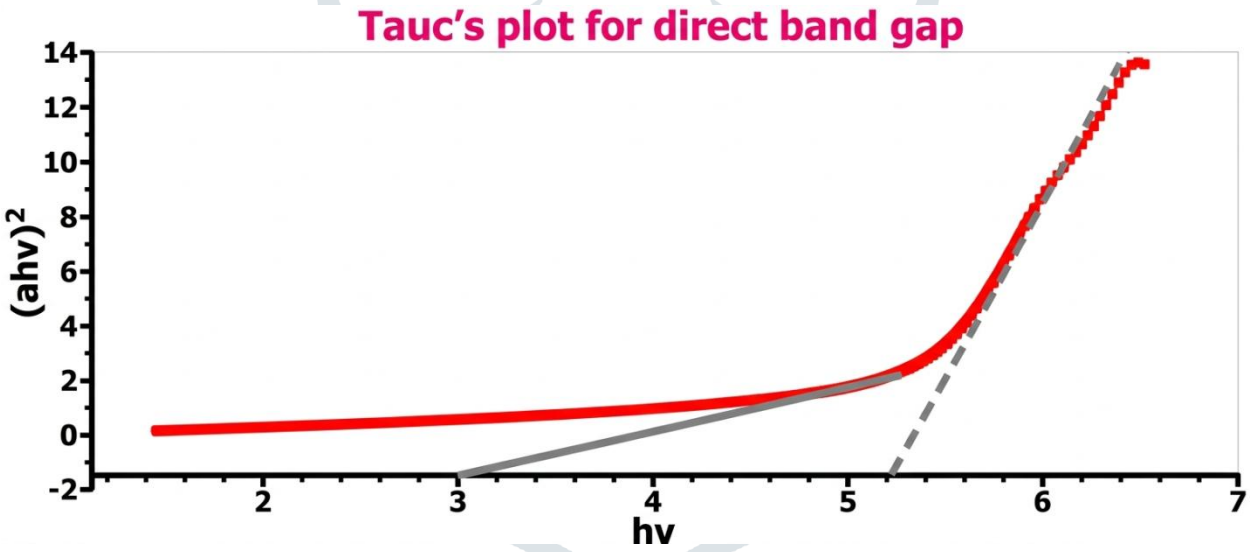

3.5 UV–Vis Spectral Comparison and Band Gap Analysis:

Figure 8 presents the comparative UV–Vis absorption spectra of *Dalbergia sissoo* leaf extract, the iron precursor ($FeSO_4$), and the synthesized iron oxide nanoparticles. The plant extract exhibited characteristic absorption features corresponding to various phytochemical constituents, whereas the iron precursor showed less absorption as compared to extract in the UV–visible region. In contrast, the γ-Fe_2O_3 nanoparticles displayed a pronounced absorption band with a noticeable spectral shift relative to both the precursor and the extract, confirming the successful biogenic synthesis of iron oxide nanoparticles. The strong absorption observed in the 200–400 nm region is attributed to electronic transitions associated with iron oxide nanostructures. Singh et al. (2020) also find similar observation of UV absorption and Rheima (2016) in their paper reported that synthesized maghemite was 21.7 nm, and their band gap was 2.49 eV.

The optical band gap energy of the synthesized iron oxide nanostructures was estimated using the Tauc relation based on UV–Vis absorption data (Johannes et al., 2020; Haryński et al., 2022; Sangiorgi et al., 2017). For the direct allowed transition, a plot of $(\alpha h\nu)^2$vs hν was employed. The indirect band gap energy was determined by extrapolating the linear region of the curve to the photon energy axis α=0 yielding a value of approximately 2.94eV, which indicates wide band gap behavior and pronounced quantum confinement effects (Diwan & Dubey, 2014; Vatankhah & Ebadi,2013).

3.6 Thin Film Electrical Study:

Figure 9: various electrical characteristics of thin film

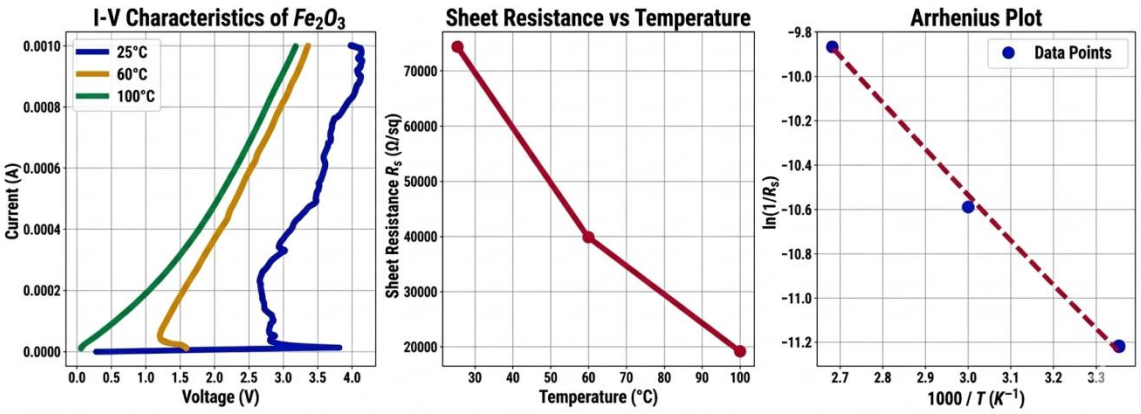

Table 1.2: relation between temperature and avg. sheet resistance.

Temperature (°C)	Condition	Avg. Sheet Resistance (Ω/sq)(Approx.)
25	Room Temperature	74500
60	at 60 degree celsius	39500
100	at 100 degree celsius	19000

The electrical properties of green-synthesized γ-Fe_2O_3 nanoparticles were investigated using the van der Pauw four-probe method (Bharadwaj, 2017) at room temperature and elevated temperatures. The I–V characteristics exhibited linear behavior, confirming ohmic conduction of the γ-Fe_2O_3 thin film under the experimental conditions. With an increase in temperature up to 100 °C, the sheet resistance decreased at an average rate of 740.6 Ω/ sq°C, demonstrating negative temperature coefficient (NTC) behavior typical of semiconducting metal oxides.

The average sheet resistance values at different temperatures are summarized in Table 1.2 The temperature dependence of resistivity obeyed the Arrhenius relation,

$$\rho\ (T) = \ \rho_o \exp\left(\frac{E_a}{kT}\right)$$

which describes thermally activated charge transport in semiconductors (Laidler, 1984). The Arrhenius plot of ln(ρ) versus 1/T yielded an activation energy (E_a) of 0.1736 eV, indicating thermally assisted conduction dominated by localized states. Such a low activation energy suggests that charge carriers require minimal thermal energy to hop between defect-related or grain-boundary states, a behavior commonly reported for nanocrystalline iron oxide thin films and nanoparticles. This behavior is consistent with a thermally activated conduction mechanism, where electrical transport occurs through hopping of charge carriers between localized states created by structural defects, oxygen vacancies, and grain boundaries. As temperature increases, the thermal energy enhances carrier mobility by facilitating hopping across these potential barriers, resulting in a decrease in resistivity and confirming semiconducting behavior of the material (Bari & Patil, 2014; Belekar, 2018; Abbas et al., 2017; Raddaoui et al., 2021).

4.Conclusion:

In the present work, γ-Fe_2O_3 (maghemite) nanoparticles were successfully synthesized through plant mediated nanoparticles synthesis method using *D. sissoo* leaf extract. XRD analysis confirmed the formation of predominantly cubic spinel γ-Fe_2O_3 with an average crystallite size of approximately **11.3 nm**, in good agreement with standard JCPDS/ICCD card no. 00-039-1346. The presence of a minor α-Fe_2O_3 phase was detected after refinement. FESEM analysis revealed quasi-spherical nanoparticles with an average particle size of **16.9 nm**, slightly larger than the XRD crystallite size, indicating single-crystalline particles may surrounded by a thin disordered surface layer. FTIR spectroscopy confirmed characteristic Fe–O vibrational modes at 618 cm^{-1} of maghemite and revealed the presence of plant-derived phytochemical as capping and reducing agents. EDS analysis further verified the elemental purity and near-stoichiometric Fe_2O_3 Fe:O 2:2.7 composition.UV–Vis spectroscopy demonstrated strong absorption in the ultraviolet region, attributed to $O^{2-} \rightarrow Fe^{3+}$

charge-transfer transitions, confirming the semiconducting nature of the synthesized nanoparticles. Optical band gap analysis revealed both direct (2.94 eV), indicating quantum confinement effects and phonon-assisted electronic transitions, which are typical for nanocrystalline iron oxide systems.

Thin films fabricated by the drop-casting method exhibited smooth, crack-free morphology, almost absence coffee ring and stable electrical behavior. Electrical characterization was done through four probes, the van der Pauw method. Linear I–V characteristics, confirming ohmic conduction. The temperature-dependent resistivity displayed a negative temperature coefficient, characteristic of semiconducting behavior. The Arrhenius analysis yielded a low activation energy of 0.1736 eV, indicating thermally activated hopping conduction through shallow localized states. This low activation energy is attributed to the nanocrystalline nature of γ-Fe_2O_3, improved crystallinity after annealing, and defect-assisted charge transport mechanisms, consistent with earlier reports on iron oxide nanostructures. So that synthesized nanomaterials can be used for applications in gas sensing, photocatalysis, and low-temperature electronic devices.

Limitations

- Present study was unable to completely eliminate the small amount of α-Fe_2O_3 presence.
- The present study did not quantify the magnetic properties.
- The present study did not use profilometry to measure film uniformity.
- There was no long-term evaluation of electrical stability due to cyclic heating.
- The present study only modelled charge transport using Arrhenius modelling.
- UV-Vis spectrum and band gap could be more refined and precise by applying baseline correction, scattering effect eliminations, savitzky-golay filteration.

Significance of the Study

This study provides a low-cost synthesis method for a Non-toxic, and Green Chemistry based Metal oxide nanoparticles from phytochemicals derived from plants to replace toxic chemical reducing agents to produce nanoparticles of controlled size, phase purity, and surface functionality. The use of thin films to produce components of flexible electronics to manufacture devices, as well as avoiding and complex vacuum based deposition techniques to produce these components is a significant achievement of the work. The electrical properties observed and measured, will support the use of the materials to fabricate devices that will assume a semiconducting device in function. The significance of this is a link between Green Chemistry and Functional Electronic Materials, with experimental verification of Sustainable Metal-oxide Electronics.

Future Scope

- Magnetic property characterization for sensor and biomedical applications.
- Gas sensing studies using controlled atmosphere and humidity levels.
- Photochemical degradation studies, utilizing both visible and solar irradiation.
- Optimum film thickness to improve transport charge will be analyzed.
- Incorporate flexible substrates for use with wearable electronic devices.
- Studies to compare each extract of your plants to others.
- Electronic device fabrication such as resistive and/or sensing components.

References:

1. Abbas, K., Atiq, S., Riaz, S., & Naseem, S. (2017). Thermally activated variations in conductivity and activation energy in $SrMnO_3$. Journal of Materials Science: Materials in Electronics, 28. https://doi.org/10.1007/s10854-017-6397-5
2. Abuzeid, H. M., Julien, C. M., Zhu, L., & Hashem, A. M. (2023). Green synthesis of nanoparticles and their energy storage, environmental, and biomedical applications. Crystals, 13(11), 1576. https://doi.org/10.3390/cryst13111576
3. Alagiri, M., & Hamid, S. B. A. (2014). Green synthesis of α-Fe_2O_3 nanoparticles for photocatalytic application. Journal of Materials Science: Materials in Electronics, 25(8), 3572–3577. https://doi.org/10.1007/s10854-014-2058-0
4. Alduhaidahawia, A., & Alantaki, A. (2025). Solar cell application via metal oxide nanoparticles. Journal of Kufa for Chemical Sciences, 5(1), 590–615. https://doi.org/10.36329/jkcm/2025/v5.i1.19845
5. Alshamsi, H. A., & Hussein, B. S. (2018). Synthesis, characterization and photocatalysis of γ-Fe_2O_3 nanoparticles for degradation of Cibacron Brilliant Yellow 3G-P. Asian Journal of Chemistry, 30(2), 273–279. https://doi.org/10.14233/ajchem.2018.20888
6. Arulkumar, E., & Thanikaikarasan, S. (2023). Physical, chemical, electronic and optical properties of CuO/NiO@n-Si thin films by drop casting method for p–n junction diode. Chemical Physics Impact, 3, 100350. https://doi.org/10.1016/j.chphi.2023.100350

7. Baig, N., Kammakakam, I., & Falath, W. (2021). Nanomaterials: a review of synthesis methods, properties, recent progress, and challenges. Materials Advances, 2(6), 1821–1871. https://doi.org/10.1039/D0MA00807A
8. Bari, R., & Patil, S. (2014). Studies on spray pyrolised nanostructured SnO_2 thin films for H_2 gas sensing application. International Letters of Chemistry, Physics and Astronomy, 36, 125–141. https://doi.org/10.18052/www.scipress.com/ILCPA.36.125
9. Bayda, S., Adeel, M., Tuccinardi, T., Cordani, M., & Rizzolio, F. (2020). The history of nanoscience and nanotechnology: From chemical–physical applications to nanomedicine. Molecules, 25(1), 112. https://doi.org/10.3390/molecules25010112
10. Belekar, R. M. (2018). Structural and electrical studies of nanocrystalline Fe_2O_3 prepared by microwave assisted solution combustion method with mixed fuel approach.Journal of Physical Sciences, 23, 189–199.
11. Bharadwaj, P. (2017). Van der Pauw resistivity measurement [Technical note]. ResearchGate. https://doi.org/10.13140/RG.2.2.23468.67208
12. Bhattacharya, M., Singh, A., & Ramrakhyani, C. (2014). *Dalbergia sissoo* – An Important Medical Plant.Journal of Medicinal Plants Studies, 2(2), 76–82. Available at https://www.plantsjournal.com/vol2Issue2/Issue_feb_2014/12.1.pdf
13. Biswas, B., Rahman, M. L., Ahmed, M. F., & Sharmin, N. (2024). Extraction of gamma iron oxide (γ-Fe_2O_3) nanoparticles from waste can: Structure, morphology and magnetic properties. Heliyon, 10(10), e30810. https://doi.org/10.1016/j.heliyon.2024.e30810
14. Boroumand Moghaddam, A., Namvar, F., Moniri, M., Md Tahir, P., Azizi, S., & Mohamad, R. (2015). Nanoparticles biosynthesized by fungi and yeast: A review of their preparation, properties, and medical applications. Molecules, 20(9), 16540–16565. https://doi.org/10.3390/molecules200916540
15. Boshoman, S. B., Fatoba, O. S., & Jen, T. C. (2023). Transition metal oxides as electrocatalytic material in fuel cells: A review. Engineered Science, 25, 948. https://doi.org/10.30919/es948
16. Darezereshki, E. (2010). Synthesis of maghemite (γ-Fe_2O_3) nanoparticles by wet chemical method at room temperature. Materials Letters, 64(13), 1471–1472. https://doi.org/10.1016/j.matlet.2010.03.064
17. Darezereshki, E., Ranjbar, M., & Bakhtiari, F. (2010). One-step synthesis of maghemite (γ-Fe_2O_3) nanoparticles by wet chemical method. Journal of Alloys and Compounds, 502(1), 257–260. https://doi.org/10.1016/j.jallcom.2010.04.163
18. Diwan, B. D., & Dubey, V. K. (2014). Influence of size on effective band gap of silicon nano-wire. Advanced Materials Research, 938, 322–326. https://doi.org/10.4028/www.scientific.net/AMR.938.322
19. Freestone, I., Meeks, N., Sax, M., & Higgitt, C. (2007). The Lycurgus Cup — A Roman nanotechnology. Gold Bulletin, 40(4), 270–277. https://doi.org/10.1007/BF03215599
20. Haryński, Ł., Olejnik, A., Grochowska, K., & Siuzdak, K. (2022). A facile method for Tauc exponent and corresponding electronic transitions determination in semiconductors directly from UV–Vis spectroscopy data. Optical Materials, 127, 112205. https://doi.org/10.1016/j.optmat.2022.112205
21. Johannes, A. Z., Pingak, R. K., & Bukit, M. (2020). Tauc plot software: Calculating energy gap values of organic materials based on Ultraviolet-Visible absorbance spectrum. IOP Conference Series: Materials Science and Engineering, 823(1), 012030. https://doi.org/10.1088/1757-899X/823/1/012030
22. Johnson, T. S., Nair, S., de'Souza, A., & Hingorani, L. (2024). Dalbergia sissoo Roxb. ex-DC. – A monograph. Pharmacognosy Reviews, 18(36), 137–150. https://doi.org/10.5530/phrev.20242024
23. Karami, H. (2010). Synthesis and characterization of iron oxide nanoparticles by solid state chemical reaction method. Journal of Cluster Science, 21(1), 11–20. https://doi.org/10.1007/s10876-009-0278-x
24. Karunakaran, G., Sudha, K. G., Ali, S., & Cho, E. B. (2023). Biosynthesis of nanoparticles from various biological sources and its biomedical applications. Molecules, 28(11), 4527. https://doi.org/10.3390/molecules28114527
25. Khezri, R., & Vahdat, S. M. (2025). Reactions and catalytic applications of metal and metal oxide nanoparticles in organic and inorganic chemistry. Inorganica Chimica Acta, 588, 122842. https://doi.org/10.1016/j.ica.2025.122842
26. Kulkarni, D., Sherkar, R., Shirsathe, C., Sonwane, R., Varpe, N., Shelke, S., More, M. P., Pardeshi, S. R., Dhaneshwar, G., Junnuthula, V., & Dyawanapelly, S. (2023). Biofabrication of nanoparticles: Sources, synthesis, and biomedical applications. Frontiers in Bioengineering and Biotechnology, 11, 1159193. https://doi.org/10.3389/fbioe.2023.1159193
27. Laidler, K. J. (1984). The development of the Arrhenius equation. Journal of Chemical Education, 61(6), 494–. https://doi.org/10.1021/ed061p494
28. Layek, S., Pandey, A., Pandey, A., & Verma, H. C. (2010). Synthesis of γ-Fe_2O_3nanoparticles by citrate precursor method. International Journal of Engineering Science and Technology, 2(8), 33–39. https://doi.org/10.4314/ijest.v2i8.63778
29. Marica, I., Stefan, M., Boca, S., Falamas, A., & Farcau, C. (2023). A simple approach for coffee-ring suppression yielding homogeneous drying patterns of ZnO and TiO2 nanoparticles. Journal of Colloid and Interface Science, 635, 117–127. https://doi.org/10.1016/j.jcis.2022.12.113
30. Morales Morales, J. A. (2017). Synthesis of hematite α-Fe_2O_3 nano powders by the controlled precipitation method. Ciencia en Desarrollo, 8(1), 99–107. https://doi.org/10.19053/01217488.v8.n1.2017.4494

31. Ogholbeyg, A., Kianvash, A., Hajalilou, A., Abouzari-Lotf, E., & Zarebkohan, A. (2018). Cytotoxicity characteristics of green assisted-synthesized superparamagnetic maghemite (γ-Fe_2O_3) nanoparticles. Journal of Materials Science: Materials in Electronics, 29. https://doi.org/10.1007/s10854-018-9321-8

32. Raddaoui, Z., El Kossi, S., Brahem, R., Bajahzar, A., Trukhanov, A. V., Kozlovskiy, A. L., Zdorovets, M. V., Dhahri, J., & Belmabrouk, H. (2021). Hopping conduction mechanism and impedance spectroscopy analyses of $La_{0.70}Sr_{0.25}Na_{0.05}Mn_{0.70}Ti_{0.30}O_3$ ceramic. Journal of Materials Science: Materials in Electronics, 32, 16113–16125. https://doi.org/10.1007/s10854-021-06160-6

33. Reibold, M., Paufler, P., Levin, A. A., Kochmann, W., Pätzke, N., & Meyer, D. C. (2006). Carbon nanotubes in an ancient Damascus sabre. Nature, 444, 286. https://doi.org/10.1038/444286a

34. Rezić, I. (2022). Nanoparticles for biomedical application and their synthesis. Polymers, 14(22), 4961. https://doi.org/10.3390/polym14224961

35. Rheima, A. (2016). Synthesis of γ-Fe_2O_3, α-Fe_2O_3 and Fe3O4 nanoparticles by electrochemical method. Journal of Chemical, Biological and Physical Sciences, 6.

36. Sale, C. S., Bhimanaboina, R., & Yu, J. (2022). Transition metal oxides for supercapacitors. In Transition Metal Oxides for Supercapacitors (pp. 267–292). Springer, Cham. https://doi.org/10.1007/978-3-030-99302-3_13

37. Sangiorgi, N., Aversa, L., Tatti, R., Verucchi, R., & Sanson, A. (2017). Spectrophotometric method for optical band gap and electronic transitions determination of semiconductor materials. Optical Materials, 64, 18–25. https://doi.org/10.1016/j.optmat.2016.11.014

38. Singh, C., Baboota, R. K., Naik, P. K., & Singh, H. (2012). Biocompatible synthesis of silver and gold nanoparticles using leaf extract of Dalbergia sissoo. Advanced Materials Letters, 3(4), 279–285. https://doi.org/10.5185/amlett.2011.10312

39. Singh, K., Chopra, D. S., Singh, D., & Singh, N. (2020). Optimization and ecofriendly synthesis of iron oxide nanoparticles as potential antioxidant. Arabian Journal of Chemistry, 13(12), 9034–9046. https://doi.org/10.1016/j.arabjc.2020.10.025

40. Singh, K., Ohlan, A., Kotnala, R. K., Bakhshi, A. K., & Dhawan, S. K. (2008). Dielectric and magnetic properties of conducting ferromagnetic composite of polyaniline with γ-Fe_2O_3 nanoparticles. Materials Chemistry and Physics, 112(2), 651–658. https://doi.org/10.1016/j.matchemphys.2008.06.026

41. Steinhauer, S. (2021). Gas sensors based on copper oxide nanomaterials: A review. Chemosensors, 9(3), 51. https://doi.org/10.3390/chemosensors9030051

42. Vatankhah, C., & Ebadi, A. (2013). Quantum size effects on effective mass and band gap of semiconductor quantum dots. Research Journal of Recent Sciences, 2(1), 21–24.

43. Yadav, P., Manori, S., Chamoli, P., Raina, K. K., & Shukla, R. K.(2023).Microwave assisted green synthesis of γ-Fe_2O_3 nanoparticles and their application for photodegradation of ternary dye mixture.Journal of Materials Science: Materials in Electronics, 34(12), 1065. https://doi.org/10.1007/s10854-023-10463-1

44. Yasmeen, S., & Gupta, P. (2021). Cosmeceutical and anticancer potential of aqueous extracts of Dalbergia sissoo Roxb. aerial parts. Journal of Herbal Medicine, 29, Article 100456. https://doi.org/10.1016/j.hermed.2021.100456